Intrasubband and intersubband transitions in lightly and heavily doped GaAs/$Al_xGa_{1-x}As$ multiple quantum wells

Qin-Sheng Zhu, X. B. Wang, Z. T. Zhong, X. C. Zhou, Y. P. He, Z. P. Cao, G. Z. Zhang, J. Xiao, X. H. Sun, and H. Z. Yang

Institute of Semiconductors, Chinese Academy of Sciences, P.O. Box 912, Beijing 100083, People's Republic of China and National Laboratory for Surface Physics, Chinese Academy of Sciences, P.O. Box 603, Beijing 100083, People's Republic of China

Q. G. Du

National Laboratory for Surface Physics, Chinese Academy of Sciences, P.O. Box 603, Beijing 100083, People's Republic of China

(Received 24 September 1996; revised manuscript received 24 September 1997)

We use a polarizer to investigate quantum-well infrared absorption, and report experimental results as follows. The intrasubband transition was observed in GaAs/$Al_xGa_{1-x}As$ multiple quantum wells (MQWs) when the incident infrared radiation (IR) is polarized parallel to the MQW plane. According to the selection rule, an intrasubband transition is forbidden. Up to now, most studies have only observed the intersubband transition between two states with opposite parity. However, our experiment shows not only the intersubband transitions, but also the intrasubband transitions. In our study, we also found that for light doping in the well (4×10^{18} cm^{-3}), the intrasubband transition occurs only in the lowest subband, while for the heavy doping (8×10^{18} cm^{-3}), such a transition occurs not only in the lowest subband, but also in the first excited one, because of the electron subband filling. Further experimental results show a linear dependence of the intrasubband transition frequency on the root of the well doping density. These data are in good agreement with our numerical results. Thus we strongly suggest that such a transition can be attributed to plasma oscillation. Conversely, when the incident IR is polarized perpendicular to the MQW plane, intersubband-transition-induced signals appear, while the intrasubband-transition-induced spectra disappear for both light and heavy well dopings. A depolarization blueshift was also taken into account to evaluate the intersubband transition spectra at different well dopings. Furthermore, we performed a deep-level transient spectroscopy (DLTS) measurement to determine the subband energies at different well dopings. A good agreement between DLTS, infrared absorption, and numerical calculation was obtained. In our experiment, two important phenomena are noteworthy: (1) The polarized absorbance is one order of magnitude higher than the unpolarized spectra. This puzzling result is well explained in detail. (2) When the IR, polarized perpendicular to the well plane, normally irradiates the 45°-beveled edge of the samples, we only observed intersubband transition spectra. However, the intrasubband transition signals caused by the in-plane electric-field component are significantly absent. The reason is that such in-plane electric-field components can cancel each other out everywhere during the light propagating in the samples. The spectral widths of bound-to-bound and bound-to-continuum transitions were also discussed, and quantitatively compared to the relaxation time τ, which is deduced from the electron mobility. The relaxation times deduced from spectral widths of bound-to-bound and bound-to-continuum transitions are also discussed, and quantitatively compared to the relaxation time deduced from electron mobility. [S0163-1829(98)01912-2]

I. INTRODUCTION

Infrared absorption due to electronic transitions between subbands in doped GaAs/$Al_xGa_{1-x}As$ multiple quantum wells (MQW's) has recently attracted considerable interest due to potential applications for infrared detection. Up to now, most studies of quantum-well infrared photodetectors have concentrated on the intersubband transition in the GaAs/$Al_xGa_{1-x}As$ material system,[1–7] in which the selection rules forbid intersubband infrared (IR) radiation into the structure. Optical gratings, usually metallic, or waveguides have been used. As an exception, Rosencher *et al.*[8] observed intrasubband photoconductivity for parallel-polarized light in GaAs/$Al_xGa_{1-x}As$ MQW's for the case of normal incidence. They attributed the intrasubband transition to a hot-electron bolometric effect. As pointed out in that work, excitation is bolometric rather than optical. Recently, Peng and Fonstad[9] also observed an intrasubband transition in δ doped $In_xGa_{1-x}As$ single quantum wells. They attributed such a transition to an intrasubband plasma oscillation, but not to hot-electron transport. In this paper, we report another intrasubband transition in GaAs/$Al_xGa_{1-x}As$ MQW's which occurs for light polarized parallel to the quantum-well plane, and also attribute this phenomenon to the intrasubband plasma oscillation mechanism. A quantitative analysis based on the plasma oscillation model will be given in detail in this paper.

In the case of light doping, we can only observe plasma oscillation in the lowest subband and 0–1 intersubband transition. For heavy doping, however, the plasma oscillation was observed to occur not only in the lowest subband but also in the upper one. Both 0–1 and 1–2 (continuum state)

intersubband transitions were observed. This paper will give a detailed analysis about this aspect.

Our measured absorption spectra reveal two distinct phenomena: (1) The scale for the polarized absorbance is one order of magnitude higher than the unpolarized absorbance [see Figs. 1(a)–1(c)]. A reasonable explanation is as follows. In the case of unpolarization, the projection of incident natural light in a typical direction will reduce the incident light intensity I_0 by half. Further projections of such light with intensity of $I_0/2$ to the x and z directions give values of $(\sin 45°)^2 I_0/2 = I_0/4$ and $(\cos 45°)^2 I_0/2 = I_0/4$, respectively. Therefore, the magnitude of absorbances for the intersubband transition caused by an electric-field component in the z direction, and for the intrasubband transition caused by x-direction component, are both less than 1 [see Fig. 1(a)], respectively. However, in the case of polarization, the projection of incident light, with an intensity $I_0/2$ (just transmitted throughout the polarizer), in the x and z directions is $I_0/4$ in all cases. Later analysis will show that the component along the x direction will be canceled out by other parallel incident light (see Fig. 2), and that the component along the z direction will be increased by the other light. Thus, the component light along the z direction can be obtained as $I_0/2$. According to the absorbance definition, we can obtain a larger value of the absorbance, which is almost one order of magnitude higher than that of the unpolarized spectra. (2) When the IR polarized perpendicular to the well plane normally irradiates the 45°-beveled edge of the samples, we only observed intersubband transition spectra. However, the intrasubband transition signals induced by the in-plane electric-field component are significantly absent. The reason considered here is that such an in-plane electric-field component can be canceled out by another parallel incident light within the samples. We will discuss the situation for some typical points in the sample, and then extend it to analyze a general case. As a result, the in-plane electric-field component is canceled out everywhere in the samples.

In addition to the above two aspects, it is also noteworthy that the spectrum, labeled A, located at wave number 1309 cm^{-1}, as shown in Fig. 4(b), which is believed to be due to the bound-to-continuum transition at heavy doping (8×10^{18} cm^{-3}), shows a spectrum half-width of 35 cm^{-1}. It is broader than those bound-to-bound transition spectra (~ 25 cm^{-1}). Before explaining peak A, we must answer the question of why those bound-to-bound transitions result in narrow spectra with half widths ~ 25 cm^{-1}. We speculate on the carrier relaxation time deduced from the Lorentzian distribution function by fitting, and from the relaxation time deduced from the mobility measured at room temperature. The former is 0.42 ps, and the latter is 0.15 ps. Two relaxation times are of the same order (subpicosecond). The difference between them can be explained as follows. At room temperature, LO-phonon scattering is the main mechanism to broaden the spectra. For the mobility, at room temperature, in addition to LO-phonon scattering, deep center scattering, and heterointerface roughness scattering, for example, can make additional contributions to the mobility. Furthermore, for the case of peak A, because the second excited state out of the well will be split into a continuum with a width of several meV, the bound-to-continuum transition spectra are wider than the bound-to-bound transition spectra.

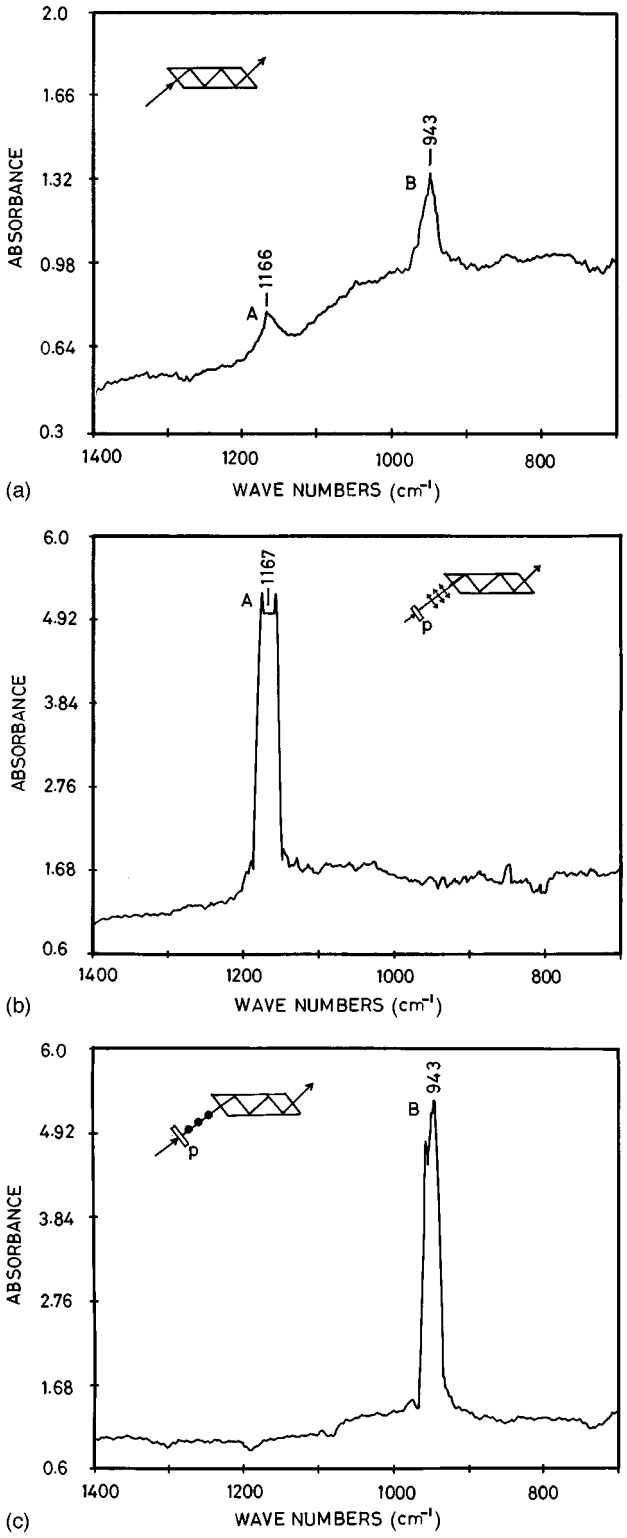

FIG. 1. Absorption spectra for a typical sample (sample 1) with doping density $N_d = 4\times10^{18}$ cm^{-3} in MQW's measured by using (a) unpolarized incident light, (b) incident light polarized perpendicular to the MQW's plane, and (c) incident light polarized parallel to the MQW's plane. In the inset, P denotes the polarizer. The scale of the vertical axis is absorbance A given by $A = \ln(I_o/I_t)$, where I_o and I_t are the intensities of the incident and transmitted lights, respectively.

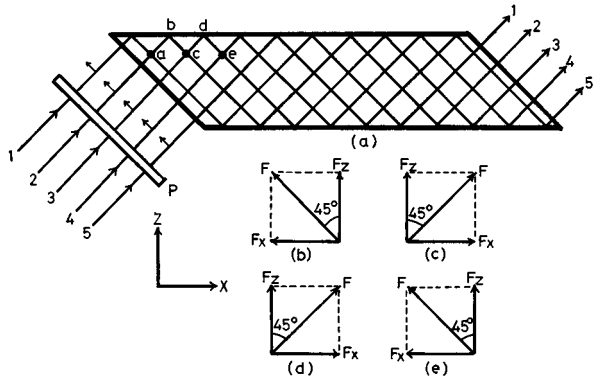

FIG. 2. (a) Schematically illustrated light passes in a sample. Five typical single lights separated by an equal distance normally irradiates the 45°-beveled sample edge. *p* denotes the polarizer. (b) and (c) show the electric fields at points *c* and *e* for light 3, respectively. (d) and (e) show the electric fields at point *c* for light 2 and at point *e* for light 4, respectively.

One may raise the question of why our absorption spectra show not only intersubband transition signals, but also intrasubband transition signals, which is very different from previous results obtained by other authors. There may be several reasons for this: (1) The unpolarized spectra due to collective excitation are very weak in magnitude, so that they may be covered up by the noise background. (2) Generally, the well doping level is 1×10^{18} cm^{-3} or less, as reported by many authors. According to our plasma model, the expected oscillation frequency is less than about 450 cm^{-1}, which is much lower than the intersubband transition frequency of 1000 cm^{-1} (corresponding to a wavelength of 10 μm). If one is careless, this spectrum, appearing on the very low-frequency side, can be hardly observed. (3) The collective excitation can be observed only in high-quality samples, as demonstrated by our many experiments.

The observation of plasma oscillation encourages us to study additional physical problems, for example, the plasma and LO-phonon interaction. Such interaction can be studied by absorption measurements performed at different temperatures. This work remains to be done in the near future. Furthermore, for application, if the plasma oscillation can give rise to lateral photocurrent, it can be used to create normal incidence photodetectors that perform at room temperature.

Because the intersubband transition energy depends strongly on the subband energy in the wells, it is necessary to perform another experiment to determine the subband positions. The deep-level transient spectroscopy (DLTS) method is a good candidate for investigating the subband energy. In the case of a square quantum well, the well itself acts as a ''giant trap'' for the DLTS measurement. This concept was first proposed in Ref. 10, and then adopted in Refs. 11 and 12 to determine the $In_xGa_{1-x}As/Al_{0.2}Ga_{0.8}As$ and $In_{0.49}Ga_{0.5}P/GaAs$ conduction- and valence-band offsets and subband energies. We extended the ''big trap'' concept from a square well to the V-shaped potential well of δ-doped GaAs to determine the subband energies,[13] and determined the *x* conduction-subband energies in a type-II GaAs/AlAs/GaAs single quantum well.[14] In this study we will use this method to demonstrate the subband energies and to compare it with numerical results and infrared-absorption data.

II. EXPERIMENT

A. Sample preparation

The samples used were grown by conventional molecular-beam epitaxy (MBE) in a VG-80H MBE system. The substrates were undoped, semi-insulating (100) GaAs. A buffer, consisting of undoped 200-nm GaAs, and 1-μm n^+-type GaAs with a Si concentration of 4×10^{18} cm^{-3}, and followed by 5-nm undoped GaAs, was grown at a substrate temperature of 690 °C. The active region, consisting of a stack of 50 quantum wells each with a width of 8 nm, separated by 40-nm-thick $Al_xGa_{1-x}As$ ($x=0.34$) barriers, was next grown at a substrate temperature of 610 °C. The wells were doped in the center 5.2 nm with Si concentrations of 4×10^{18} and 8×10^{18} cm^{-3}, respectively, for observing the plasma oscillation in the lowest excited subbands in the wells. The samples were capped by 5 nm of undoped GaAs and finally by 0.4 μm of *n*-type GaAs for infrared-absorption and DLTS measurements. For the latter measurement, gold Schottky barriers with an area of 3×10^{-2} cm^2 were formed by evaporation.

B. Measurements

Absorption spectra are measured at room temperature using a Fourier transform infrared spectrometer. The samples are typically 4 mm long and 0.4 mm thick, and have their ends beveled at 45°. In this case, nine double passes are made through these quantum wells as the light passed down the length of the samples. The scan of the incident light covers a wave number range from 700 (14.3 μm) to 1400 cm^{-1} (7.1 μm). A polarizer is introduced to polarize the incident infrared light. The light is polarized parallel or perpendicular to the plane of the quantum well to measure intrasubband and intersubband transitions, respectively. The fabricated diodes typically have a leakage current of 0.2 μA at reverse bias 0–6 V. The DLTS measurements are carried out with a high sensitivity system which can detect a minimum deep level concentration down to 5×10^{12} cm^{-3}. The temperature scan covers a temperature range 77–400 K. At the quiescent bias, total wells are out of but quite near the depletion region edge, so at the reverse bias (-3 V), all wells are active for DLTS measurement. In order to determine the subband energies and subband populations in MQW's, the frequency of output pulse is changed from 26 to 2600 Hz to obtain the subband energies (''giant trap'' activation energies).

III. THEORETICAL CONSIDERATIONS

Considering an *n*-type GaAs quantum well with an effective well width of d^* in the well, the electrons act as a two-dimensional plasma. Such a plasma can be considered an anisotropic slab with an effective thickness d^* and a spatially uniform effective dielectric tensor with principal components[15]

$$\varepsilon_x(\omega)=\varepsilon_x\left[1-\frac{4\pi n_s e^2}{\varepsilon_x m_x d^*\omega(\omega+i\gamma_x)}\right], \tag{1}$$

$$\varepsilon_z(\omega)=\varepsilon_z+\sum_{ij}\frac{4\pi n_s e^2 f_{ij}}{m_{ij}d^*(\omega_{ij}^2-\omega^2-i\gamma_{ij}\omega)}, \tag{2}$$

$$\varepsilon_y(\omega)=\varepsilon_x(\omega), \tag{3}$$

where x, y, and z are the directions of propagation of the modes. x and y axes are defined to be parallel to the quantum-well plane, and the z axis is parallel to the growth direction (because the x-y plane is parallel to the well, the choice of x and y axes used in the present case is arbitrary). γ_x is the damping constant of the carriers for motion in the x or y direction. ε_x, ε_y, and ε_z are the optical dielectric constants parallel and perpendicular to the quantum-well plane in the GaAs active layers, respectively ($\varepsilon_x=\varepsilon_y$). f_{ij}, ω_{ij} and γ_{ij} are the oscillator strength, frequency and damping constant of the i-j intersubband electronic excitations.

The longitudinal plasma eigenmodes (plasmons) are obtained from

$$\varepsilon(q,\omega)=0, \tag{4}$$

that is,

$$\varepsilon_y(q,\omega)=\varepsilon_x(q,\omega)=0, \tag{5}$$

$$\varepsilon_z(q,\omega)=0. \tag{6}$$

For multiple-layered interacting plasmons associated with several zero-thickness two-dimensional electron gas (2DEG) layers separated by spacer layers of thickness d, it has been shown that the plasmon frequency is[16]

$$\omega_x^2=\frac{n_s e^2 q_{xy}}{2\varepsilon_0\varepsilon_x m_x^*}S(q_{xy},q_z), \tag{7}$$

where the structure factor S is given by

$$S(q_{xy},q_z)=\frac{\sinh(q_{xy}d)}{\cosh(q_{xy}d)-\cos(q_z d)},$$

where q_{xy} is the in-plane wave vector, and q_z is the wave vector normal to the quantum wells. In the strong-coupling limit, i.e., $q_{xy}d\ll 1$ (in the present case, the in-plane wave vector is $q_{xy}\sim(2\pi/\lambda)<10^4$ cm^{-1},[17] where the incident light wavelength λ is about 10 μm, and the well thickness $d=8.2\times10^{-7}$ cm), the electron-electron density oscillation along the z direction constitutes a 3D-like q_z plasmon for a 2DEG of finite thickness [$q_z\sim10^4$ cm^{-1}, which can be regarded as $q_z\sim0$ (Ref. 17)]. The initial p'_{xy} and final p_{xy} electron momenta in the plane of the quantum wells are related by the conservation law $p_{xy}=p'_{xy}+hq_{xy}$, $q=(q_{xy},q_z)$. At the Brillouin-zone edge, the wave vector is $2\pi/a\cong10^8$ cm^{-1}, where a is the GaAs lattice constant (5.6 Å). Comparing to this value, q_{xy} is negligibly small ($\sim10^4$ cm^{-1}), that is, it is very close to the Brillouin-zone center. Thus, to a good approximation, the in-plane electron momenta conservation law becomes $p_{xy}=p'_{xy}$. Summing up the above analysis, Eq. (7) becomes

$$\omega_x^2=\frac{4\pi N_d e^2}{m_x^*\varepsilon_x}. \tag{8}$$

This is a 3D plasmon, with an effective 3D electron density $N_d=n_s/d^*$, where d^* is the effective well width. m_x^* is the electron effective mass in a different subband in the x direction. Due to the subband-filling effect, the carrier densities in 0 and 1 subbands are different, which obeys the Fermi distribution function. Furthermore, we assume that the value of the optical dielectric constant ε_x is no different between the 0 and 1 subbands.[18]

Letting d be the well width and d^* the effective well width, and defining a ratio $\xi=d^*/d$,[19] the plasma frequency can be rewritten as

$$\omega_x^2=\frac{4\pi N_d e^2}{m_x^*\xi\varepsilon_x}, \tag{9}$$

where N_d is the 3D average doping density given by $N_d=n_s/d$. In the case of infinite barrier height, $\xi=0.58$,[19] while in the case of finite barrier height, $0.58<\xi<1$.

If the incident wave includes an electric-field component of E_z in the z direction (perpendicular to the quantum-well plane), the electric radiation field can be coupled to the z-direction oscillation mode, and provides wave energy to the plasma oscillation. When $E=E_{ij}^*$, plasma resonance in the z direction will occur, and then an absorption peak can be observed at this frequency. On the other hand, if the incident wave has an electric-field component E_x, the radiation field can be coupled to the x-direction oscillation mode, and provides wave energy to the x-direction plasma oscillation. When $E=E_x$, resonance in the x direction will occur, and then the absorption peak can be observed at the energy E_x.

To deal with the intersubband transition problem, one has to add an effective plasma energy term E_p^2 to the bare transition energy E_{ij}^2. Then the frequency of the collective intersubband mode can be expressed as

$$E_{ij}^{*2}=E_{ij}^2+E_p^2, \tag{10}$$

where

$$E_p^2=\frac{8\pi n_s e^2 E_{ij}L_{ij}}{\varepsilon_x}. \tag{11}$$

In Eq. (11) L_{ij} is the Coulomb matrix element,[20,21] that describes the depolarization shift. It is given by

$$L_{ij}=\int dx\left[\int \psi_j(x')\psi_i(x')dx'\right]^2. \tag{12}$$

$\psi_i(x)$ and $\psi_j(x)$ are the envelope functions of the two subbands.

In polar semiconductors like GaAs, collective intersubband excitations are coupled to optical phonons, and the coupled-mode frequencies are given by[22,23]

$$1-\frac{E_{\rm TO}^2-E_\pm^2}{E_{\rm LO}^2-E_\pm^2}\times\frac{E_p^2}{E_\pm^2-E_{ij}^2}=0, \tag{13}$$

where $E_{\rm LO}$ and $E_{\rm TO}$ are the energies of LO and TO phonons. The solution of Eq. (13) is

$$E_{\pm}^2=\frac{E_{ij}^2+E_{\mathrm{LO}}^2+E_p^2}{2} \pm\frac{\sqrt{(E_{ij}^2+E_{\mathrm{LO}}^2+E_p^2)^2-4(E_{ij}^2E_{\mathrm{LO}}^2+E_{\mathrm{TO}}^2E_p^2)}}{2}. \tag{14}$$

In our study, the intersubband transition energy E_{ij} (E_{01} or E_{12}) is more than 100 meV, and E_{LO} is only $\sim$36 meV. Thus $E_{ij}\gg E_{\mathrm{LO}}$. In this case, the high-energy mode is $E_+=E_{ij}^*$, which can be observed from experiment.

IV. RESULTS AND DISCUSSION

A. Light doping in quantum wells

To reveal the absorption spectra clearly, we carefully draw the spectra from the original data without any correction, and show them in Figs. 1 and 4. In these figures, the background of the polarized spectra is much flatter than that of unpolarized spectra, like the background absorption spectra reported by Peng and Fonstad.[9] We measured many samples, and found the same behavior.

Figure 1(a) shows the absorption spectra from a typical sample (sample 1) containing 50 Si-doped (4×10^{18} cm^{-3}) quantum wells at room temperature without using a polarizer. Two peaks, labeled A and B, are observed at wave numbers 1166 cm^{-1} (corresponding to wavelength 8.6 μm) and 943 cm^{-1} (10.6 μm), respectively. However, when the incident wave is polarized perpendicular to the quantum-well plane, only one absorption peak A appears, as shown in Fig. 1(b). On the other hand, when the incident light is polarized parallel to the quantum-well plane, only one absorption peak B appears, as shown in Fig. 1(c), in which the absorption peak A completely disappears. In order to identify the origin of peak A, we calculated the subband energies in the well. For the GaAs/Al$_x$Ga$_{1-x}$As system, the band gap of Al$_x$Ga$_{1-x}$As is given by $E_g=(1.424+1.247x)$ eV (in the present case, $x=0.34$) at 300 K. Using the ratio of $\Delta E_c/\Delta E_g=0.60$, we obtain the band offset $\Delta E_c=0.254$ eV. The plane-wave extension method was used to calculate the lowest and first excited subband energies. The first ten extended plane waves were adopted to calculate the subband energy values approximately. Many researchers have used the plane-wave extension method to calculate the subband energies because of its accuracy. More recently, our group successfully used this method to determine subbands in the MQW's to evaluate absorption spectra broadening. One will see that, throughout this paper, we use this method to calculate subband energies which agree well with the experimental data. In the present case, by using this method, the energies of the two subbands in the wells are 46 and 171 meV above the bottom of the well, respectively. Taking into account the E_p contribution, good agreement between the expected and measured results is obtained. Thus we propose that peak A corresponds to the 0–1 intersubband transition. For peak B, we can calculate the plasma frequency ω_x by using Eq. (9). With $N_d=4\times10^{18}$ cm^{-3}, $\varepsilon_x=10.2$,[24] and $\xi=0.68$ for the Al molar fraction of $x=0.34$, we obtain 10.8 μm for the plasma wavelength. This value is in good agreement with the measured value of 10.6 μm. The small deviation may be attributed to the fact that the true Si-doping density is slightly higher than the designed value of 4×10^{18} cm^{-3} in the GaAs active layers. If so, the plasma oscillation peak would appear on the short-wavelength side.

We also measured another ten samples with different well widths and Al molar fraction x, and found that they show the same behavior. The positions of peaks A and B for a sample with the same well width, Al molar fraction x, and doping density are very close to each other. As can be seen in Figs. 1(a), 1(b), and 1(c), the polarized absorbance is one order of magnitude higher than the unpolarized spectra. This phenomenon is also observable in Figs. 4(a), 4(b), and 4(c). Let us now explain these results. When the incident light normally irradiates the 45°-beveled sample side (without using a polarizer), the wave vector of the electric field of the incident light is well distributed in all directions (0°–360°). If such lights project in a typical direction, the incident light intensity I_0 will decrease to $I=I_0/2$. Furthermore, we decompose the I to $I(\sin 45°)^2=I_0/4$ along the x direction and to $I(\cos 45°)^2=I_0/4$ along the z direction, respectively; then the absorbance A can be expressed as

$$A=\ln\frac{I_0}{I_t}=\ln\frac{I_0}{I_0-I_0\beta/4}=\ln\frac{4}{3}=0.29, \tag{15}$$

where I_t is the transmitted light intensity, and the introduced parameter β is the quantum efficiency which describes electron and incident photon interaction. β is very close to unity. For the light doping sample ($n=4\times10^{18}$ cm^{-3}), Fig. 1(a) gives the absorbance $A=0.16$ for peak A and $A=0.37$ for peak B, respectively. These data are in good agreement with our simple prediction given by Eq. (15).

Conversely, when the incident light polarized within the x-z plane normally irradiates the 45°-beveled sample edge [see Fig. 2(a)], the intensity of such polarized light decreases to $I=I_0/2$ (I_0 is the incident light intensity). Furthermore, decomposition of this light in x and z directions gives intensities of $I_x=(\sin 45°)^2I_0/2=I_0/4$ and $I_z=(\cos 45°)^2I_0/2=I_0/4$, respectively. I_x can be canceled out by other parallel incident light [see Fig. 2(a)], i.e., $I_x+(-I_x)=0$, and I_z can be summed up by this parallel incident light, i.e., $I_z+I_z=I_0/2$. Details will be given in the next paragraph. Assuming that the incident light is mostly absorbed by electrons in the wells, the absorbance A can be obtained as

$$A=\ln\frac{\frac{I_0}{2}}{\frac{I_0}{2}-\beta\frac{I_0}{2}}=\ln\frac{1}{1-\beta}. \tag{16}$$

When the quantum efficiency $\beta=0.99$, the absorbance $A=4.6$, and when $\beta=0.999$, $A=6.9$. This result can be compared to our experimental data as shown in Figs. 1(b) and 1(c) and 4(b) and 4(c).

From the description of the experiment and the schematic insets to Figs. 1(a)–1(c) and 4(a)–4(c), it is apparent that while 100% in-plane polarization of the electric-field component of the incident light can be obtained, the maximum perpendicular polarization is only 50%. The component of the parallel polarization is nonzero but also 50%. However,

we can hardly find an in-plane plasma oscillation in Figs. 1(b) and 4(b). In order to explain this phenomenon, we schematically illustrate light passes in some detail in Fig. 2. Experimentally, the incident light can be regarded as many parallel single lights. For the sake of simplicity, we draw only five typical lines separated by an equal distance, as shown in Fig. 2(a). These lights, with the same frequency ω and initial phase angle θ_0, can be expressed as $F=F_0\exp[i(\omega t-\mathbf{kr}+\theta_0)]$, where the incident lights polarized perpendicular to the quantum wells normally irradiate the sample at the 45°-beveled side. In Fig. 2(a), we can see that the distance between positions a and b, b and c, c and d, and d and e are all the same. Thus the phase angles at points a, c, and e are all the same. In addition, according to optical reflection theory, after light reflection at the interface between the medium and air, the phase angle will change π. Taking this aspect into account, the electric fields found at points c and e for line 3 have an opposite component of electric field F_x's along the x direction, as shown in Figs. 2(b) and 2(c). At the same time, the electric fields at point c for line 2 and at point e for line 4, as shown in Figs. 2(d) and 2(e), can completely cancel out the F_x's at points c and e for line 3, respectively. On the other hand, the upward electric-field components will be added to one another at points c and e. As a result, the electrons can only absorb the electric-field component perpendicular to the MQW's, but cannot absorb that parallel to the MQW's. The same analysis is also valid for any point within the sample, as shown in Fig. 2(a). Therefore, we can only observe signals which stem from the intersubband transition, as shown in Figs. 1(b) and 4(b).

As shown in Figs. 1(c) and 4(c), when the incident radiation is polarized parallel to the quantum wells, we can clearly observe the absorption spectra believed to be due to the intrasubband transition. This implies that normal incidence can also cause such a transition. In order to confirm this idea, we performed a normal-incidence experiment on the same sample to observe the absorption signal. As a result, a weak spectrum at wave number 943 cm^{-1} [which is same as peak B in Fig. 1(a)] with the same spectrum half-width was observed. In this study, we used a waveguide approach rather than a normal-incidence method to realize strong absorption.

Finally, to confirm the origin of peak B in Fig. 1(a), several samples with the same structure but different doping densities were measured. Figure 3 shows the experimental data. We find that the frequency of peak B is linearly proportional to the root of the carrier concentration. This result is strong evidence to support our point of view: that peak B stems from the intrasubband plasma oscillation.

We are now in a position to discuss what is different here compared to the work of Rosencher *et al.*,[8] who used a normal incidence to observe an intrasubband transition, and attributed it to the hot-electron bolometric effect. However, they did not discuss the hot-electron signal as a function of doping density. When we consider the doping, the hot-electron bolometric effect fails in explaining our data. Whereas, if we use a collective excitation mechanism to state our experimental results, we find that the plasma frequency ω_x is proportional to the root of doping density, as shown in Fig. 3. We also used our plasma oscillation mechanism to explain the experimental results of Ref. 8 tentatively. In Ref. 8, the GaAs well widths were 6 nm, with a Si doping density

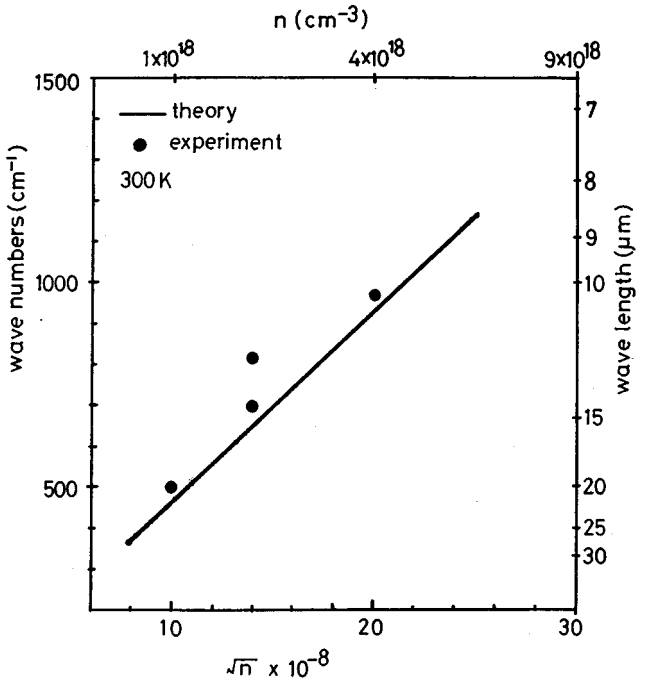

FIG. 3. Wave numbers of peak B measured from several samples with the same structure but different doping densities as a function of root doping density in quantum wells. The solid line is calculated using Eq. (9).

$n_s=5\times10^{11}$ cm^{-2} (corresponding to $N_d=0.83\times10^{18}$ cm^{-3}). According to Eq. (9), the predicted plasma oscillation wavelength is 24.9 μm (corresponding to wave number 401 cm^{-1}). However, Rosencher *et al.* observed an absorption peak at $\lambda=10.2$ μm. This experimental value is much lower than the predicted plasma wavelength. It is also worth noting that the measurement performed by Rosencher *et al.* was at a much lower temperature of 15 K, while our measurement was done at 300 K. In addition, our spectra are much different from these of Ref. 8 in shape. It is apparent that the absorption observed by Rosencher *et al.* was not based on collective excitation. On the other hand, our absorption result also cannot be explained by the hot-electron bolometric effect. Therefore, we believe that plasma oscillation is a more reasonable mechanism than the hot-electron bolometric effect to analyze our experimental results.

B. Heavy doping in quantum wells

When the Si-doping density increases to 8×10^{18} cm^{-3}, the absorption spectra are much different from that of light doping in quantum wells. Figure 4(a) shows the measured absorption signals without using a polarizer. Five peaks, labeled A, B, C, D, and E, located at wave numbers 1309 (7.7 μm), 1207 (8.3 μm), 988 (10.1 μm), 968 (10.3 μm), and 847 cm^{-1} (11.8 μm), respectively, are observed. When the incident wave is polarized perpendicular to the quantum-well plane, only three absorption peaks A, B, and C are left, as shown in Fig. 4(b). On the other hand, when the incident light is polarized parallel to the quantum-well plane, another two absorption peaks D and E are left, whereas peaks A, B, and C completely disappear, as shown in Fig. 4(c).

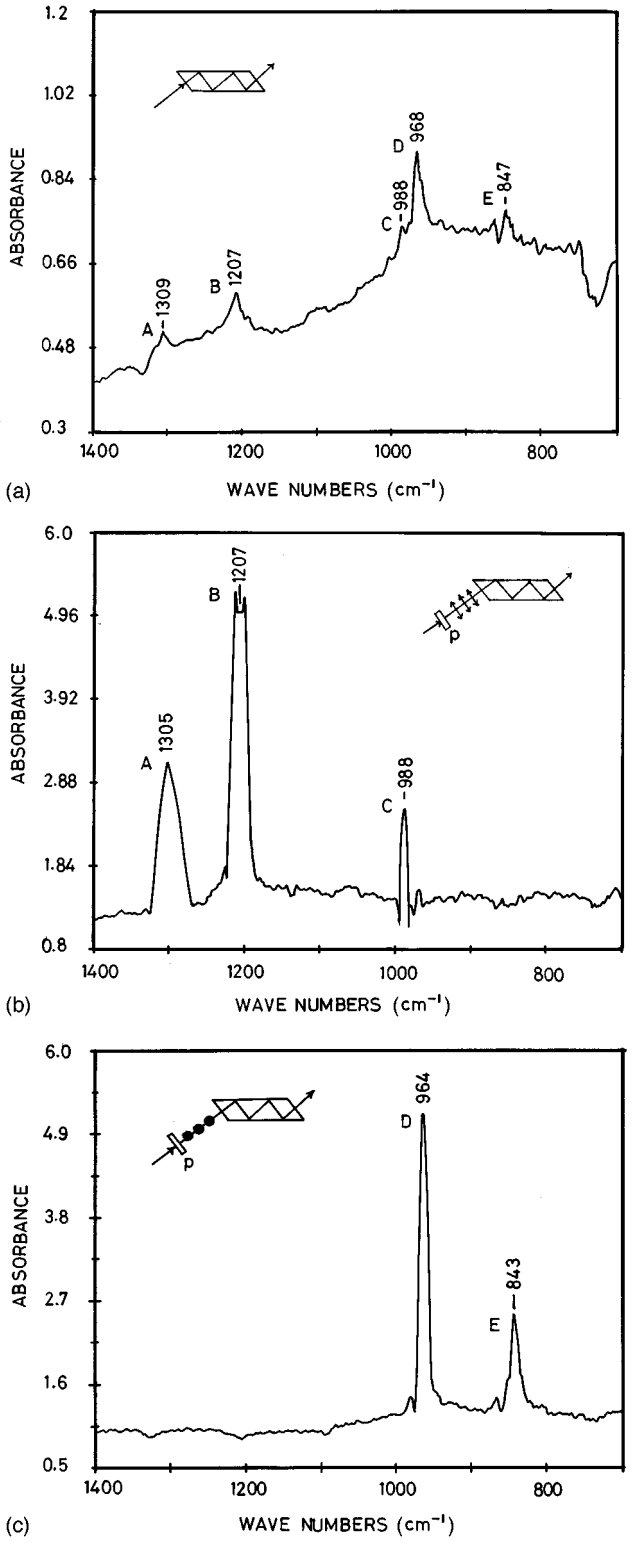

FIG. 4. Absorption spectra for a typical sample (sample 2) with doping density 8×10^{18} cm^{-3} in MQW's measured by using the (a) unpolarized incident lights, (b) incident light polarized perpendicular to the quantum-well plane, and (c) incident light polarized parallel to the quantum-well plane. In the inset, P denotes the polarizer.

Let us now analyze the width of the intersubband transition spectra. As shown in Figs. 1(b) and 4(b), the 0–1 intersubband transition spectra all exhibit the narrow full width at half maximum (FWHM) of ~25 cm^{-1} for both light and heavy doping. The intersubband transition spectra can be well fitted by the Lorentzian distribution function, which is given by

$$L=\frac{1}{\pi}\frac{\hbar/\tau}{(E_1-E_0-\hbar\omega)^2+(\hbar/\tau)^2} \tag{17}$$

where τ is the carrier relaxation time. By letting $E_1-E_0-\hbar\omega=0$, the maximum Lorentzian is

$$L=\frac{1}{\pi}\frac{\tau}{\hbar}. \tag{18}$$

The energy separation between the center and half maximum of the Lorentzian is $E_1-E_0-\hbar\omega=2\pi c\hbar k_h=1.55$ meV, where the wave number $k_h=\mathrm{FWHM}/2=12.5$ cm^{-1}. Then we obtain

$$\frac{1}{2}L=\frac{1}{\pi}\frac{\hbar/\tau}{(2\pi c\hbar k_h)^2+(\hbar/\tau)^2}. \tag{19}$$

Both Eqs. (18) and (19) give a result of $\tau=0.42$ ps. On the other hand, the electron mobility μ for our heavily doped samples measured at room temperature is about 4000 cm^2/V s. From $\mu=(e/m^*)\tau$, a value of $\tau=0.15$ ps can be obtained. The relaxation time τ deduced from the spectra is about three times as large as that obtained from the mobility. There may be several factors that broaden the absorption spectra: (1) carrier lifetime, (2) nonparabolicity of the in-plane 2D conduction subbands, (3) fluctuation of the thickness of the well, and (4) LO-phonon scattering. Among them, LO-phonon scattering is the major mechanism to reduce the carrier relaxation time. Nonparabolic broadening can be neglected because the depolarization effect compensates for the line distortion induced by different curvatures of the subband. In the case of mobility, we must consider additional scattering processes. They are (1) ionized impurity scattering, (2) deep center scattering, (3) neutral impurity scattering, (4) deformation potential scattering, (5) piezoelectric scattering, (6) heterointerface roughness scattering, and other unknown scattering processes. The scattering mechanisms for the electron mobility are more numerous than those for spectra broadening processes. On the other hand, at room temperature, LO-phonon scattering is the main mechanism to broaden the spectra. However, in the case of mobility, at room temperature, in addition to the LO-phonon scattering, other scattering, for example, deep center scattering and heterointerface roughness scattering, also make some contribution to mobility. (The influence of heterointerface roughness on mobility is more considerable than that on the absorption spectra broadening.) Thus it is reasonable to propose that the relaxation time τ deduced from the mobility is lower than that speculated from optical broadening. We turn now to peak A. Peak A in Fig. 4(b), with a FWHM of about 35 cm^{-1} is wider than others (25 cm^{-1}). This implies that in addition to the scattering-induced spectra broadening, as discussed above for bound-to-bound transition, we have to take into account the second-excited-state broadening. Because this state is out of the well, it will be split into the continuum. Therefore, spectrum A must be wider than the others. We

refer the reader to Ref. 25 for further results on the bound-to-continuum transition spectra width.

At the next step, we consider the intersubband transition at room temperature. Prior to doing this, we have to determine the Fermi levels at light and heavy doping in the well. For light doping (4×10^{18} cm^{-3}), the Fermi level is in the minigap between E_0 and E_1. In this case, we use the equation

$$n_s=\int_0^\infty D_2F(E)dE, \tag{20}$$

where the sheet doping density n_s is given by $N_d\times d=3.2\times10^{12}$ cm^{-2}. D_2 is the 2D density of state given by $m^*/\pi\hbar^2$, and $F(E)$ is the Fermi distribution function. The solution of Eq. (20) is

$$E_{FL}=kT\ \ln\left[\exp\left(\frac{\pi\hbar^2n_s}{m^*kT}\right)-1\right]. \tag{21}$$

The subscript L denotes the light doping. This equation gives a value of $E_F=114$ meV above the bottom of the well. This value is 69 meV higher than E_0, so the lowest subband can be populated by all the electrons, while the first excited subband can be populated by negligible electrons. On the other hand, for heavy doping (8×10^{18} cm^{-3}), the Fermi level is above the E_1 level. In this case, the 0 subband is filled up with electrons, and the first excited state, with a density of state of $2m^*/\pi\hbar^2$, which is twice as high as D_2 appearing in Eq. (20), is expressed as follows:

$$n_s=\int_{E_0}^{E_1}D_2dE+\int_{E_1}^{\infty}2D_2F(E)dE. \tag{22}$$

The solution is

$$E_{FH}=kT\ \ln\left\{\exp\left[\frac{\pi\hbar^2}{2m^*kT}\times\left(n_s-\frac{m^*}{\pi\hbar^2}(E_1-E_0)\right)\right]-1\right\}+E_1, \tag{23}$$

where the subscript H denotes the heavy doping. Equation (23) gives the result $E_F=223$ meV, which is 52 meV higher than E_1 (171 meV). By using the Fermi energy $E_F-E_1=52$ meV for the heavy doping at room temperature, $F(300\ \mathrm{K})=0.88$. Therefore, the population for the lowest state is $N_0=N_d/(1+0.88)=4.26\times10^{18}$ cm^{-3}, and that for the first excited state is $N_1=0.88N_d/(1+0.88)=3.74\times10^{18}$ cm^{-3}. Considering the contribution of the energy E_p to E_{01}^*, the value of 1208 cm^{-1} (8.3 μm) is close to the experimental value 1207 cm^{-1} (8.3 μm). Because of the subband filling effect, in addition to the 0–1 transition, the subband 1 to continuum state transition will occur. The absorption coefficients for 0–1 and 1–2 (continuum state) subband transitions appear as follows:

$$\alpha_{01}(\omega)=A_1\int d^2k\ F(E_0)[1-F(E_1)]L_1(E_1-E_0-\hbar\omega), \tag{24}$$

$$\alpha_{12}(\omega)=A_2\int d^2k\ F(E_1)L_2(E_2-E_1-\hbar\omega), \tag{25}$$

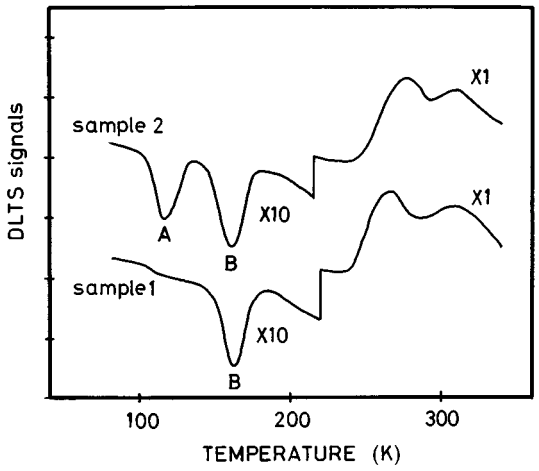

FIG. 5. DLTS signals measured from sample 1 with doping density 4×10^{18} cm^{-3}, and sample 2 with 8×10^{18} cm^{-3} in the MQW's. For sample 1, only one signal, labeled B, due to electron emission from the lowest subband to the $Al_xGa_{1-x}As$ conduction band, appears. For sample 2, in addition to peak B, peak A also appears, which is due to electron emission from the first excited subband to the $Al_xGa_{1-x}As$ conduction band.

with

$$L_1=\frac{1}{\pi}\frac{\hbar/\tau_1}{(E_1-E_0-\hbar\omega)^2+(\hbar/\tau_1)^2}, \tag{26}$$

$$L_2=\frac{1}{\pi}\frac{\hbar/\tau_2}{(E_2-E_1-\hbar\omega)^2+(\hbar/\tau_2)^2}, \tag{27}$$

where F is the Fermi distribution function, and k is the vector perpendicular to the growth axis. $E_0(k)$, $E_1(k)$, and $E_2(k)$ give the dispersion relations perpendicular to the growth axis for the 0 and 1 subbands and continuum states. τ_1 and τ_2 are the relaxation times which were discussed at length previously. A_1 and A_2 are the proportionality factors including the dipole matrix elements, respectively. The absorption coefficient α_{12} is smaller than α_{01}. Peak C, with a small absorption amplitude at 988 cm^{-1}, shown in Fig. 4(b) may be due to one or two quantum wells with well widths larger than the designed value during the growth process.

We now turn to the intrasubband transitions. Using Eq. (9), the predicted plasma frequency for peak D is 905 cm^{-1} which is close to the measured value of 968 cm^{-1}, and that for peak E is 849 cm^{-1}, which is very close to measured data at 843 cm^{-1}. The measured spectra are shown in Fig. 4(c).

C. DLTS results

To identify the subband population, a DLTS measurement was performed on lightly and heavily doped samples. Figure 5 shows these results. For a doping density of 4×10^{18} cm^{-3} (sample 1), only one signal, peak B, with an activation energy of 0.23 ± 0.02 eV below the top of the well, can be seen. When the well doping density increases to 8×10^{18} cm^{-3} (sample 2), in addition to signal B, peak A, with an activation energy of 0.11 ± 0.02 eV, appears. These activation energies for signals A and B are very close to the

calculated subband energies, which are 0.21 and 0.09 eV below the top of the wells for 0 and 1 subbands. We further repeat the DLTS measurements with Schottky diodes made on the same sample after removing the MQW's by chemical etching. Peaks *A* and *B*, believed to be due to quantum-well emission, are significantly absent. Though the experimental results have some uncertainty, the measured activation energies are in good agrement with the caculated subband energies.

V. CONCLUSION

In conclusion, we observed intersubband and intrasubband transitions in $GaAs/Al_xGa_{1-x}As$ MQW's with light and heavy Si doping, when the incident light is polarized in directions perpendicular and parallel to the quantum-well plane. The suggested mechanism, intrasubband collective excitation, is supported by an important experimental fact: the plasma frequency is linearly proportional to the root of doping density in MQW's. In the case of light doping (4×10^{18} cm^{-3}), we need only take into account the intrasubband transitions in the lowest subband. In the case of heavy doping (8×10^{18} cm^{-3}), however, in addition to the lowest subband, the plasma oscillation in the first excited subband was also observed due to the upper subband filling. The agreement between the experiment and the calculation results was obtained. The subband energy levels identified by DLTS measurement can be compared with the calculation results and the absorption data on the same samples.

ACKNOWLEDGMENTS

This work was supported by the Beijing Municipal Natural Science Foundation, and by the Natural Science Foundation of China (NSFC).

[1] B. F. Levine, C. G. Bethea, V. O. Shen, and R. J. Malik, Appl. Phys. Lett. **57**, 383 (1990).
[2] Larry S. Yu and Sheng S. Li, Appl. Phys. Lett. **9**, 1332 (1991).
[3] C. G. Bethea, B. F. Levine, V. O. Shen, R. R. Abbott, and S. Hseih, IEEE Trans. Electron Devices **38**, 1118 (1991).
[4] A. Zussman, B. F. Levine, J. M. Kuo, and J. de Jong, J. Appl. Phys. **70**, 5101 (1991).
[5] B. F. Levine, G. Hasnain, C. G. Bethea, and Naresh Chand, Appl. Phys. Lett. **54**, 2704 (1989).
[6] G. Hasnain, B. F. Levine, S. Gunapala, and Naresh Chand, Appl. Phys. Lett. **57**, 608 (1990).
[7] B. F. Levine, C. G. Bethea, G. Hasnain, V. O. Shen, E. Pelve, R. R. Abbott, and S. J. Hsieh, Appl. Phys. Lett. **56**, 851 (1990).
[8] E. Rosencher, E. Martinet, E. Bockenhoff, Ph. Bois, S. Delaitre, and J. P. Hirtz, Appl. Phys. Lett. **58**, 2589 (1991).
[9] L. H. Peng and C. G. Fonstad, Appl. Phys. Lett. **63**, 1534 (1993).
[10] P. A. Martin, K. Meehan, P. Gavrilovic, K. Hess, N. Holonyak, Jr., and J. Coleman, J. Appl. Phys. **54**, 4689 (1983).
[11] N. Debbar, D. Biswas, and P. Bhattacharya, Phys. Rev. B **40**, 1058 (1989).
[12] D. Biswas, N. Debbar, P. Bhattacharya, M. Razeghi, M. Defour, and F. Omnes, Appl. Phys. Lett. **56**, 834 (1990).
[13] Q. S. Zhu, Z. T. Zhong, L. W. Lu, and C. F. Li, Appl. Phys. Lett. **65**, 2425 (1994).
[14] Qin-Sheng Zhu, Z. Q. Gu, Z. T. Zhong, Z. Q. Zhou, and L. W. Lu, Appl. Phys. Lett. **67**, 3593 (1995).
[15] W. P. Chen, Y. J. Chen, and X. Burstein, Surf. Sci. **58**, 2589 (1967).
[16] A. C. Tselis and J. J. Quinn, Phys. Rev. B **29**, 3318 (1984).
[17] D. Olego, A. Pinczuk, A. C. Gossard, and W. Wiegmann, Phys. Rev. B **25**, 7867 (1982). See also A. Pinczuk and G. Abstreiter, in *Light Scattering in Solids V*, edited by M. Cardona and G. Gunterodt (Springer-Verlag, Berlin, 1989), p. 156.
[18] P. von Allmen, M. Berz, G. Petrocelli, F-K Reinhart, and G. Harbeke, Semicond. Sci. Technol. **3**, 1211 (1988).
[19] T. Ando and S. Mori, J. Phys. Soc. Jpn. **47**, 1518 (1979).
[20] S. J. Allen, Jr., D. C. Tsui, and B. Vinter, Solid State Commun. **20**, 425 (1976).
[21] D. A. Dahl and L. J. Sham, Phys. Rev. B **16**, 651 (1977).
[22] A. Pinczuk and J. M. Worlock, Surf. Sci. **113**, 69 (1982).
[23] G. Abstreiter, in *Molecular Beam Epitaxy and Heterostructures*, edited by L. L. Chang and K. Ploog (Nijhoff, Dordrecht, 1985), p. 425.
[24] M. J. Kane, M. T. Emeny, N. Apsley, C. R. Whitehouse, and D. Lee, Semicond. Sci. Technol. **3**, 722 (1988).
[25] Y. P. He, Q. S. Zhu, Z. T. Zhong, G. Z. Zhang, Y. T. Xing, J. Xiao, Z. P. Cao, X. H. Sun, and H. Z. Yang (unpublished).